2013 IEEE/RSJ International Conference on
Intelligent Robots and Systems (IROS)
November 3-7, 2013. Tokyo, Japan

# Leg Stiffness Adaptation for Running on Unknown Terrains

Bruce D. Miller, David Cartes and Jonathan E. Clark

*Abstract*— **The ability of biological locomotors to rapidly and stably traverse unstructured environments has inspired the development of numerous legged robotic platforms. While strides have been made in negotiating terrains cluttered with obstacles, dealing with surface property variations has received less consideration. This work presents a leg stiffness control strategy that estimates the surface compliance and adjusts the leg stiffness in order to maintain a nominal locomotion behavior while allowing for stable transitions between surfaces of up to three orders of magnitude differences in ground compliance. Implementation of this technique with high-bandwidth variable stiffness actuators that are currently being developed will expand the range of legged robotic platforms to environments with sudden and significant changes in terrain characteristics.**

## I. Introduction

Animals have demonstrated the ability to run quickly, nimbly, and stably across environments with numerous obstacles and rapidly changing surface properties. In an effort to improve our understanding of the principles contributing to high-speed, biological locomotion, reduced-order models, such as the spring loaded inverted pendulum (SLIP) model, were developed [1]. Though the governing equations of motion for this model are quite simple, the resulting center of mass trajectory and ground reaction force profiles closely match those of a wide variety of animals [2]. Analysis of this model and its dynamics has yielded insights into the role of passive system properties, such as leg stiffness and body mass, in achieving stable and efficient locomotion. This has led to its use as a template for the design and control of several legged robotic platforms [3]–[5].

While robotic instantiations have demonstrated the utility of the SLIP model in the design of legged locomotors, the performance of these platforms is limited when compared to their biological counterparts. While animals have been shown to traverse obstacles and transition between terrains with minimal impact on their locomotion dynamics [6], [7], few legged platforms have demonstrated the capacity to cross environments with any sort of unanticipated obstacles [8]. Furthermore, changes in ground properties, such as compliance and traction, have been shown to adversely affect the performance of dynamic legged robots, resulting in significantly decreased efficiency and stability [9].

Observations of humans running have shown that when faced with ground stiffness variations, we tend to alter our effective leg stiffness. This is done to maintain a consistent total-system compliance [10]. For example, a person running on a soft surface stiffens his legs, while a person running on a hard surface will relax his legs to be more compliant. This allows individuals to utilize similar locomotion dynamics when traversing a variety of terrains that would naturally be encountered. Recent investigations on the role of compliance in robotic leg design have corroborated these results, indicating that tuning leg stiffness can improve running performance on robotic systems, often to a greater extent than tuning controller parameters [9], [11].

Insights as to the impact of leg stiffness on running performance have motivated the development of several mechanisms for stiffness adaptation on running platforms, ranging from mechanical solutions [12]–[15] to smart material approaches [16]–[18]. While order-of-magnitude stiffness variations have been demonstrated with these devices, only recently have such mechanisms allowed for high-bandwidth variations. Furthermore, usage of these devices is currently restricted to off-line optimization of the desired leg stiffness for specific conditions due to a lack of suitable real-time control strategies [19]. This imposes significant limitations on their use in natural environments, particularly when the surface properties are unknown or varying.

In this work, we develop a control strategy which enables legged systems to overcome abrupt and unanticipated transitions between terrains of different compliances using adaptation of the leg stiffness. This approach is based on adaptive leg parameter estimation techniques. We demonstrate that this strategy is able to rapidly and accurately estimate the appropriate leg stiffness to preserve system dynamics following a surface compliance perturbation. Furthermore, we show that by adapting the robot's leg stiffness, a nominal gait can be maintained without any variation of actuation control for changes in ground stiffness of up to three orders of magnitude.

The remainder of this paper is organized as follows. In Section II, the SLIP model is reviewed. We discuss the parameters of the model, the dynamic equations governing its motion, and basic motion followed over the course of a stride. Section III presents a control strategy for use on a SLIP-like system. This is a two-fold approach, with an energy modulation controller being used to rapidly stabilize the gait while leg stiffness adaptation maintains the system stiffness, preserving the nominal locomotion dynamics. Section IV describes the simulation methodology and the studies used to examine the stability of the controller, followed by the results of these studies and a discussion thereof. Section V summarizes insights drawn from the results and suggests applications for this approach as well as avenues for future inquiries.

B. Miller, D. Cartes, and J. Clark are with the Department of Mechanical Engineering, FAMU/FSU College of Engineering, Tallahassee, FL, USA 32301 {bdmiller, dcartes, jeclark}@fsu.edu

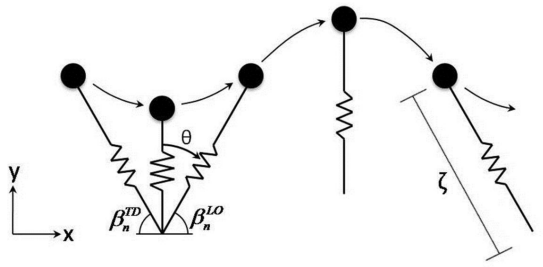


Fig. 1. Depiction of the SLIP model and a sample trajectory for a single stride. The variables $\zeta$ and $\theta$ are the coordinates that characterize the radial and angular position of the point-mass during the stance phase. The variables $x$ and $y$ are the coordinates used to characterize the horizontal and vertical position of the point-mass during the flight phase. The variables $\beta_n^{TD}$ and $\beta_n^{LO}$ show method by which the touch-down and lift-off angles are measured.

## II. The Spring Loaded Inverted Pendulum Model

The spring loaded inverted pendulum (SLIP) model has been widely used to describe the sagittal plane dynamics of legged running animals and robots. To capture the dynamics of multi-legged animals, the model uses a virtual leg that acts as the sum of all legs that would be in contact with the ground at any given instant [2]. In its simplest formulation, the SLIP model consists of a point-mass $m$ that sits atop a massless leg. The leg is typically modeled as an axially elastic, transversely rigid linear spring with a stiffness of $k$ and a nominal length of $l_0$.

Locomotion dynamics captured by the SLIP model are restricted to the sagittal plane and are shown in Fig. 1. For the purpose of this discussion, subscripts denote the stride number, while superscripts denote touch-down (TD) and lift-off (LO) events. Each stride begins with a touch-down event, which starts the stance phase. At touch-down, the leg is extended to its nominal length and contacts the ground at an angle $\beta_n^{TD}$, measured clockwise from the horizontal inertial axis to the leg axis. At this instance, the point-mass has a horizontal velocity of $\dot{x}_n^{TD}$ and a vertical velocity of $\dot{y}_n^{TD}$. Additionally, a foot-pivot is established and acts as a moment-free pin joint about which the leg rotates while in the stance phase. During the first half of stance, the leg compresses under the momentum of the point-mass and gravity. During the second half of stance, the leg extends, returning the stored elastic potential and resulting in a lift-off event, beginning the flight phase. The lift-off event occurs when the ground reaction force in the leg returns to zero, at which point the leg is at an angle $\beta_n^{LO}$, measured counter-clockwise from the horizontal inertial axis to the leg axis. During the flight phase, the body is governed by simple ballistic dynamics. The flight phase ends with the next touch-down event, which occurs when the leg, extended to its nominal length, contacts the ground at an angle $\beta_{n+1}^{TD}$.

In the conservative formulation of the SLIP model, the governing equations can be derived quite simply for both stance and flight phases. As shown in Fig. 1, when the model is in stance, a polar coordinate frame $(\zeta, \theta)$ with the origin at the foot-pivot is used, while the Cartesian inertial frame $(x, y)$ is used to describe the point-mass motion during flight. The variable $\zeta$ corresponds to the leg length, while the variable $\theta$ denotes the angle between the leg axis and the vertical inertial axis. For stance, equations of motion are derived from the Lagrangian

$$L = \frac{m}{2}\left(\dot{\zeta}^2 + \zeta^2\dot{\theta}^2\right) - mg\zeta\cos\theta - \frac{k}{2}(\zeta - l_0)^2, \quad (1)$$

which, by using Lagrange's equation, yields

$$\begin{aligned} \ddot{\zeta} &= \zeta\dot{\theta}^2 - g\cos\theta - \frac{k}{m}(\zeta - l_0) \\ \zeta\ddot{\theta} &= -2\dot{\theta}\dot{\zeta} + g\sin\theta. \end{aligned} \quad (2)$$

The flight dynamics, governed by simple ballistic motion, can be simply written as

$$\begin{aligned} \ddot{x} &= 0 \\ \ddot{y} &= g, \end{aligned} \quad (3)$$

where $g$ is the gravitational acceleration acting on the system.

## III. Control Approach

The emphasis of the control approach presented in this paper is to demonstrate the capacity of leg stiffness adaptation to restore and maintain consistent running performance when transitioning between terrains of radically different surface characteristics. However, since the general formulation of the SLIP model only demonstrates marginal stability and has a relatively small basin of attraction, an energy modulation controller is used in tandem with the leg stiffness controller to provide a wider basin and to rapidly stabilize the system once the system stiffness has settled.

### A. Energy Modulation Control

The energy modulation controller utilized is the Active Energy Removal (AER) controller, which has been verified to improve stability of running both in simulation and on a physical platform [20]. This controller was motivated by studies of leg function in insects and guinea fowl, which demonstrated that animals tend to use their muscles to perform negative work (i.e. braking) during parts of the stride [21] and that leg actuation is likely prescribed in a feed-forward manner to improve stability when faced with unanticipated obstacles [22]. These insights resulted in the formulation of a feed-forward controller that varied the force-free leg length over the course of a stride, given as

$$l(t) = l_0 - l_{dev}\sin\frac{\pi t}{t_{des}}, \quad (4)$$

where $l$ is the force-free leg length, $l_{dev}$ is the maximal variation from the nominal leg length $l_0$, $t$ is the time passed since the touch-down event, and $t_{des}$ is a timing control parameter that specifies the stance time for the nominal gait. In addition to improving the rate of convergence following a perturbation, this controller also results in asymptotic stability of the SLIP model since it is nonconservative.

A secondary element of this controller is a control law that allows for variations in leg touch-down angle $\beta_{n+1}^{TD}$, given by

$$\beta_{n+1}^{TD} = \beta_n^{LO} + c\left(\beta_n^{TD} - \beta_{des}^{TD}\right), \quad (5)$$

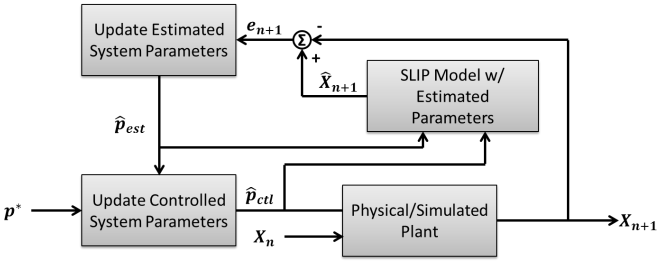


Fig. 2. Block diagram depicting the control strategy utilized to adapt the leg stiffness during each stride. The variables in the figure are described in Table I.

TABLE I

NOTATION FOR THE LEG STIFFNESS ADAPTATION STRATEGY

| Variables | |
|---|---|
| $X_n$ | System state |
| $\hat{X}_n$ | Estimated system state |
| $e_n$ | Error in estimated state |
| $\hat{p}_{est}$ | Estimated system parameters |
| $\hat{p}_{ctl}$ | Updated system parameters |
| $p^*$ | Nominal system parameters |
| **Parameters** | |
| $K_n^S$ | Estimated system stiffness |
| $K_n^G$ | Estimated ground stiffness |
| $K_n^L$ | Updated leg stiffness |
| $K_{nom}^S$ | Nominal system stiffness |
| $\gamma$ | Adaptive control gain |

where $\beta_n^{LO}$ is the previous lift-off angle, $\beta_n^{TD}$ is the previous touch-down angle, $\beta_{des}^{TD}$ is the desired touch-down angle, and $c$ is a nondimensional control parameter. This control law increases the breadth of the basin of attraction since it helps keep gaits that are rapidly converging from overshooting the nominal trajectory by pitching too far at lift-off or approaching touch-down too steeply [23].

### B. Leg Stiffness Control

Since the AER controller is able to attract gaits from a wide basin, the aim of the leg stiffness controller is solely to maintain a nominal set point of the effective system stiffness, which will allow the system dynamics and AER controller to generate the desired gait. The approach utilized to accomplish this task is similar to the strategy used by Uyanik, et al. [24]. In that study, the authors used an adjustment technique based on Kalman filtering to estimate system properties, including stiffness, that may be time-varying or poorly calibrated. We build off of this approach to include both environment and system parameters. A block diagram depicting the control approach utilized in this paper is shown in Fig. 2. The variables and parameters necessary for this approach are compiled and defined in Table I.

This strategy performs a once-per-step estimation of the system and ground stiffnesses, $K_n^S$ and $K_n^G$, respectively, and updates the leg stiffness $K_n^L$ to maintain a nominal system stiffness $K_{nom}^S$. The system stiffness is defined as the effective stiffness of the overall system resulting from adding the leg and ground springs in series. Adaptation of the stiffness parameters is based on the error in the estimated and measured states at the touch-down event $e_n$. The measured and estimated system states, $X_n$ and $\hat{X}_n$, respectively, are composed of the horizontal and vertical velocities at touch-down, $\dot{x}_n^{TD}$ and $\dot{y}_n^{TD}$, respectively, and the leg touch-down angle $\beta_n^{TD}$ of the plant. The measured system state can be determined from either the SLIP model with the actual environmental parameters or from measurements of the physical plant. The estimated state is computed via simulation of the SLIP model using the estimated system parameters.

The goal of this control approach is to minimize the difference between estimated and measured system states at touch-down. This results in an accurate estimation of the system and ground stiffnesses, which is in turn utilized to set the leg spring to the stiffness. This stiffness value is determined such that the system stiffness is maintained at its nominal value. The parameter adjustment strategy used to accomplish this task adjusts the estimate of system stiffness based on the sensitivity of the estimated SLIP model to system stiffness perturbations using

$$K_{n+1}^S = K_n^S + \gamma \left( \frac{\partial \hat{X}}{\partial K^S} \right)^{-1} \Bigg|_{\hat{X}_n} e_{n+1}, \tag{6}$$

where $K_{n+1}^S$ and $K_n^S$ are the next and current system stiffness estimates, $\gamma$ the adaptive control gain, $\frac{\partial \hat{X}}{\partial K^S}$ is a measure of the states' sensitivity to stiffness variation, and $e_{n+1}$ is the states' error from the nominal behavior. This approach is akin to the update stage of Kalman filter estimatation. Note that the partial derivative is computed numerically by imparting infinitesimal perturbations to the system stiffness and observing the resulting impact on the estimated SLIP model.

From this estimate of system stiffness, the estimated ground stiffness can be found via

$$K_{n+1}^G = \frac{K_n^L K_{n+1}^S}{K_n^L - K_{n+1}^S}. \tag{7}$$

This estimate of ground stiffness and the nominal system stiffness can be used to determine the desired leg stiffness to be used during the next stride via

$$K_{n+1}^L = \frac{K_{n+1}^G K_{nom}^S}{K_{n+1}^G - K_{nom}^S}. \tag{8}$$

Both (7) and (8) can be simply derived by assuming a series configuration of the leg and ground springs that result in the effective spring that influences the dynamics of the system.

## IV. PERFORMANCE EVALUATION

The performance of the adaptive leg stiffness controller was examined via two methods. First, a stability analysis was performed to quantify the local stability of the ground stiffness estimation as a function of the adaptive control gain $\gamma$ and the ground stiffness $K^G$. Second, the response to significant variations in ground stiffness was examined to determine the capacity of the controller to maintain

TABLE II

PARAMETERS FOR THE SLIP MODEL AND PLANT.

| Property | Value | Units |
|---|---|---|
| $m$ | 2.11 | $kg$ |
| $K^S_{nom}$ | 1.90 | $kNm^{-1}$ |
| $l_0$ | 0.298 | $m$ |
| $l_{dev}$ | 0.020 | $m$ |
| $t_{des}$ | 0.118 | $s$ |
| $\beta^{TD}_{des}$ | 1.3 | $rad$ |
| $c$ | 0.35 | – |
| $v^{TD}_{nom}$ | 2.841 | $ms^{-1}$ |
| $\delta^{TD}_{nom}$ | 1.011 | $rad$ |

stable and convergent gaits when encountering sudden and significant terrain transitions.

A SLIP simulation was developed in MATLAB, which numerically integrated the equations of motion from (2) and (3) using the Runge-Kutta integrator, *ode45*, with a tolerance of $1\times10^{-8}$. Since both leg and ground stiffnesses are considered within this simulation, $k$ is replaced with $K^S_n$ to account for both parameters. This simulation was used to determine the trajectories of both the plant and estimated SLIP models. Note that in a hardware instantiation of this control approach, the plant would be measured as the physical system rather than simulated. The physical parameters and energy modulation control parameters were set to values listed in Table II, as well as $v^{TD}_{nom}$ and $\delta^{TD}_{nom}$, the nominal velocity magnitude at and heading angle, measured clockwise from the positive x-axis, at touch-down, respectively. The physical parameters were derived from dynamically scaling [25] a human runner to $1/3$ its size by length, such that the parameters matched those of a single legged hopping robot that has been used to verify the accuracy of this simulation [20]. The energy modulation control parameters chosen were identified in previous studies to result in rapid stabilization to their nominal trajectory [26].

The results in Fig. 3 demonstrate the effectiveness of the adaptive leg stiffness control strategy in restoring the system dynamics following a change in ground stiffness. In this example, the simulated model encounters a three order-of-magnitude decrease in ground stiffness, equivalent to a 16% decrease in the effective system stiffness, during the 10th stride. When the leg stiffness adaptation algorithm is not utilized (Fig. 3A), the system diverges from the nominal trajectory, eventually resulting in system failure. However, by using the adaptive leg stiffness controller (Fig. 3B), the system returns to the nominal gait after several strides. Fig. 3C portrays the leg stiffness of the model and the estimate of the ground stiffness. This demonstrates the controller's ability to adapt the leg stiffness to preserve the nominal system stiffness, as well as the accuracy and rapid convergence in estimating the ground stiffness.

### A. Local Stability Analysis

In the first parameter variation experiment, the local stability of the controller was determined by computing the maximum eigenvalue $\lambda_{max}$ of the ground stiffness estimate, which measures the local convergence rate of the system.

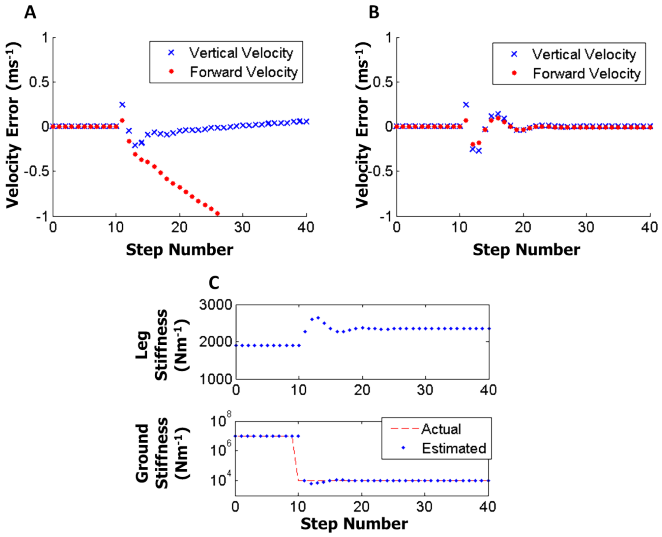


Fig. 3. Comparison of the system when utilizing leg stiffness adaptation to the system without leg stiffness control. (A) and (B) show the difference in the touch-down velocity from the nominal gait without and with the adaptive leg stiffness controller implemented, respectively. Both systems encounter a terrain transition at the 10th stride, decreasing the ground stiffness from $1\times10^7$ Nm$^{-1}$ to $1\times10^4$ Nm$^{-1}$. (C) shows the adaptation of the leg stiffness and the estimation of the ground stiffness as well.

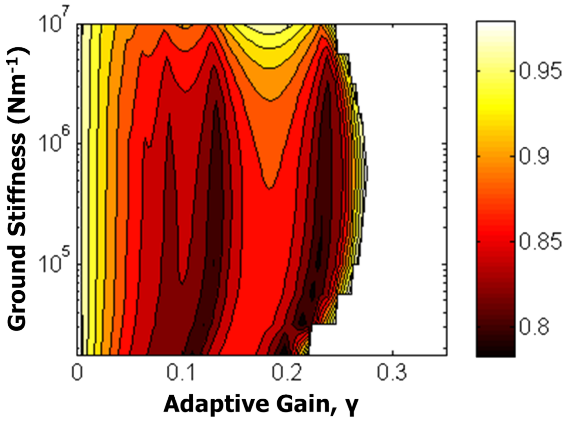


Fig. 4. Plot of the maximum eigenvalues for the convergence of the ground stiffness estimate. The colored regions show stable convergence of the ground stiffness estimate, while the white regions were unstable. The shading represents the magnitude of the eigenvalue, with dark shades showing more rapid convergence than light shades.

This analysis serves a dual purpose. First, it characterizes the range of adaptive control gains and initial ground stiffnesses for which the ground stiffness estimation converges to the actual ground stiffness. Second, it quantifies the rate at which the ground stiffness estimate converges, enabling the selection of an adaptive control gain that most rapidly converges given knowledge of the expected ground stiffness perturbations. To determine the maximum eigenvalue, the parameter space for the adaptive control gain and initial ground stiffness was discretized into 1668 parameter sets. The minimum ground stiffness considered was $10^4\ Nm^{-1}$ because below this threshold, the required leg stiffness rapidly increased and approached infinity. The maximum ground stiffness considered was $10^7\ Nm^{-1}$ since above this value, changes in

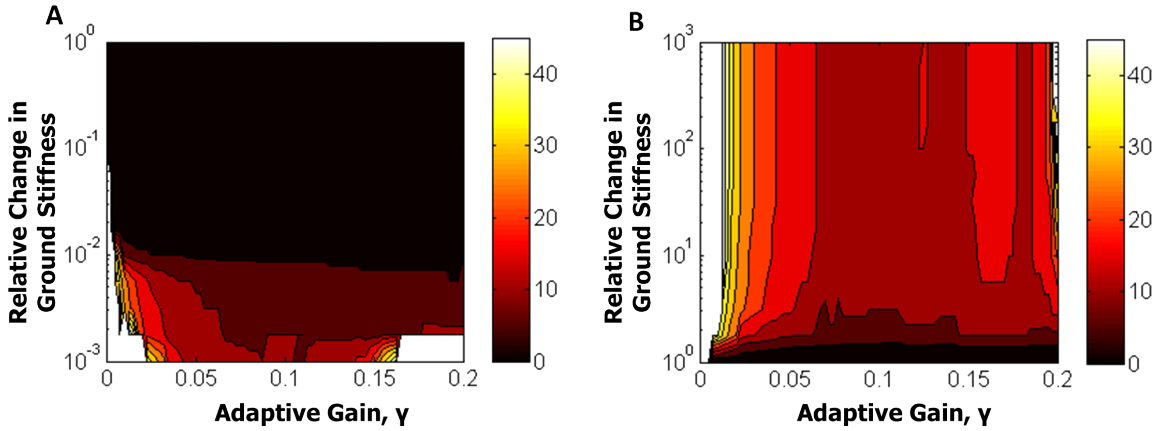


Fig. 5. Number of strides required following a terrain stiffness change to return to the nominal gait. The colored region show the parameter sets that returned to the nominal trajectory, while the white regions either fell or had not converged after 50 strides. The shading shows the number of strides required to restore the nominal gait, with dark shades returning more rapidly than light shades. (A) shows the results of encountering a decrease in stiffness of up to three orders of magnitude from an initial ground stiffness of $1 \times 10^7$ Nm$^{-1}$. (B) shows the results of encountering an increase in stiffness of up to three orders of magnitude from an initial ground stiffness of $1 \times 10^4$ Nm$^{-1}$.

ground stiffness had an insignificant effect on the effective system stiffness. Furthermore, the range of ground stiffnesses considered spanned commonly encountered surfaces, ranging from soft rubber to thick steel plates. For each parameter set, the maximum eigenvalue was determined by finding the rate of decay of the convergence envelope for the ground stiffness estimates after receiving a ground stiffness perturbation of 0.1% of the ground stiffness.

The results of this parameter sweep are shown in Fig. 4. As seen in the figure, for the majority of the parameter space, the ground stiffness estimate is locally stable ($\lambda_{max} < 1$). Furthermore, two separate regions appear to exist that exhibit the fastest convergence rates. Both of these regions demonstrate similar eigenvalue magnitudes over a comparable range of ground stiffnesses. These results indicate that the selection of an adaptive control gain in either region will result in similar convergence rates for a wide range of ground stiffnesses. However, the expected range of ground stiffnesses needs to also be considered, since on extremely rigid surfaces or compliant surfaces, the rightmost region becomes unstable.

### *B. Response to step transitions*

The second experiment examined the rate at which the system returns to the nominal trajectory following a step transition of the terrain stiffness. This investigation serves to quantify the combined ability of the adaptive leg stiffness controller and AER controller to restore the nominal gait. Both transitions from rigid to compliant surfaces and compliant to rigid surfaces were considered. As with the previous experiment, the parameter space was discretized, this time for the adaptive control gain and percentage change in ground stiffness resulting in 1053 parameter sets. For each trial, the simulation was run for 50 strides following the ground stiffness perturbation and the number of strides before the system returned to and remained within 1% of the nominal trajectory was recorded. For trials in which the initial ground height variation did not perturb the system beyond 1%, the number of strides taken to converge was set to 0; for those in which the system had still not converged after 50 strides, the system was considered to be unstable.

The results of this experiment are shown in Fig. 5. As with the maximum eigenvalue analysis, the system is able to stably recover in the majority of parameter sets examined. When encountering a decrease in ground stiffness (Fig. 5A), the system is able to recover the nominal gait within 15 strides for 92% of the cases tested. While impressive, this result is slightly misleading since a ground stiffness decrease of 2 orders of magnitude results in just a 2% change in the effective system stiffness. However, even when only considering cases in which the ground stiffness is decreased between two and three orders of magnitude (corresponding to a 2% to 16% change in system stiffness), 76% of the cases still recover the nominal gait within 15 strides. When encountering an increase in ground stiffness (Fig. 5B), the system does not recover quite as rapidly, with only 66% of the cases returning to the nominal gait within 15 strides. However, a careful selection of the adaptive control gain (i.e choosing $0.07 < \gamma < 0.14$), yields rapidly converging gaits across the entire three order-of-magnitude range of stiffness variations. It should be noted that without leg stiffness adaptation ($\gamma = 0$), the system is only stable for a single order-of-magnitude decrease in ground stiffness (it is unstable for all increases in ground stiffness) and cannot recover its nominal gait.

## V. Conclusions

In this paper, we present a leg stiffness adaptation strategy for use in stabilizing dynamic hopping when faced with variations in terrain properties. The controller operates by estimating the ground stiffness and controlling the leg stiffness to drive the system towards a nominal system stiffness. We demonstrate the effectiveness of this approach in preserving the locomotion dynamics and nominal hopping trajectory even when encountering abrupt and severe changes in ground

stiffness. Additionally, we show the capacity of the controller to accurately and rapidly estimate the ground stiffness.

The controller is shown to provide stable and accurate estimates of the ground stiffness across a wide range of ground stiffnesses, from $1 \times 10^7$ $\text{Nm}^{-1}$ to $1 \times 10^4$ $\text{Nm}^{-1}$. In addition to establishing the local convergence of stiffness estimates and locomotion dynamics across this range of surfaces, the ability to restore a nominal trajectory when encountering ground stiffness variations of up to three orders of magnitude is demonstrated.

Future investigations will consider several extensions of this work. First, the utility of the controller on a physical platform needs to be verified. As mentioned before, several mechanisms already exist to modulate leg stiffness and would be capable of implementing this controller *in situ*. Second, an extension of the controller to estimate and adapt to damping variations, in addition to stiffness, would greatly expand the potential utility of the controller. This is vital to the implementation in real-world situations since damping is significant in many terrains, especially natural environments that legged robots are geared towards navigating. In addition to determining the terrain properties and maintaining locomotion dynamics, the controller could be extended to determine 'safe' terrains, where 'safe' terrains are those that the platform is capable of adapting to. This would warn the platform that it would be unable to maintain the nominal system stiffness and the terrain should be avoided or a different gait needs to be utilized.

The success of the controller in estimating ground stiffness provides another potential role for the controller in classifying terrains. This could be used to improve the convergence to the nominal gait through the use of learning algorithms. Additionally, characterization could alert the system of hazardous terrain, such as low friction on ice, and alter the nominal gait to allow for safe traversal of such environments. Developments in these areas will results in the improved ability of legged robots to navigate unstructured terrains and begin to close the gap in locomotion performance between these robots and the animals that have inspired them.

## ACKNOWLEDGMENTS

This work was supported by the collaborative participation in the Robotics Consortium sponsored by the U.S. Army Research Laboratory under the Collaborative Technology Alliance Program, Cooperative Agreement DAAD 19-01-2-0012. The U.S. Government is authorized to reproduce and distribute reprints for Government purposes not withstanding any copyright notation thereon.

## REFERENCES

[1] R. Blickhan, "The spring-mass model for running and hopping," *Journal of Biomechanics*, vol. 22, no. 11–12, pp. 1217–1227, 1989.

[2] R. Blickhan and R. Full, "Similarity in multilegged locomotion: Bouncing like a monopode," *Journal of Comparative Physiology A-Sensory Neural and Behavioral Physiology*, vol. 173, no. 5, pp. 509–517, Nov 1993.

[3] R. Altendorfer, N. Moore, H. Komsuoglu, M. Buehler, H. Brown, D. McMordie, U. Saranli, R. Full, and D. Koditschek, "RHex: A biologically inspired hexapod runner," *Autonomous Robots*, vol. 11, pp. 207–213, 2001.

[4] I. Poulakakis, J. Smith, and M. Buehler, "Modeling and experiments of untethered quadrupedal running with a bounding gait: The Scout II robot," *The International Journal of Robotics Research*, vol. 24, no. 4, pp. 239–256, Apr 2005.

[5] S. Kim, J. E. Clark, and M. R. Cutkosky, "iSprawl: Design and tuning for high-speed autonomous open-loop running," *The International Journal of Robotics Research*, vol. 25, no. 9, pp. 903–912, 2006.

[6] S. Sponberg and R. J. Full, "Neuromechanical response of musculoskeletal structures in cockroaches during rapid running on rough terrain," *Journal of Experimental Biology*, vol. 211, no. 3, pp. 433–446, 2008.

[7] D. Ferris, M. Louie, and C. Farley, "Running in the real world: Adjusting leg stiffness for different surfaces," *Proceedings of the Royal Society of London. Series B: Biological Sciences*, vol. 265, no. 1400, pp. 989–994, 1998.

[8] K. Galloway, G. Haynes, B. Ilhan, A. Johnson, R. Knopf, G. Lynch, B. Plotnick, M. White, and D. Koditschek, "X-RHex: A highly mobile hexapedal robot for sensorimotor tasks," University of Pennsylvania, Tech. Rep., 2010.

[9] J. Jun and J. Clark, "Dynamic stability of variable stiffness running," in *Robotics and Automation (ICRA), 2009 IEEE International Conference on*, May 2009, pp. 1756–1761.

[10] D. Ferris and C. Farley, "Interaction of leg stiffness and surface stiffness during human hopping," *Journal of Applied Physiology*, vol. 82, no. 1, pp. 15–22, 1997.

[11] K. Galloway, J. Clark, M. Yim, and D. Koditschek, "Experimental investigations into the role of passive variable compliant legs for dynamic robotic locomotion," in *Robotics and Automation (ICRA), 2011 IEEE International Conference on*, May 2011, pp. 1243–1249.

[12] K. Galloway, J. Clark, and D. Koditschek, "Design of a multi-directional variable stiffness leg for dynamic running," *Mechanics of Solids and Structures Parts A and B*, vol. 10, pp. 73–80, 2007.

[13] K. Hollander, T. Sugar, and D. Herring, "Adjustable robotic tendon using a 'Jack Spring'$^{TM}$," in *Rehabilitation Robotics (ICORR), 9th International Conference on*, 2005, pp. 113–118.

[14] J. Hurst, J. Chestnutt, and A. Rizzi, "The actuator with mechanically adjustable series compliance," *Robotics, IEEE Transactions on*, vol. 26, no. 4, pp. 597–606, Aug 2010.

[15] L. Visser, R. Carloni, and S. Stramigioli, "Energy-efficient variable stiffness actuators," *Robotics, IEEE Transactions on*, vol. 27, no. 5, pp. 865–875, 2011.

[16] Y. Chen, J. Sun, Y. Liu, and J. Leng, "Variable stiffness property study on shape memory polymer composite tube," *Smart Materials and Structures*, vol. 21, no. 9, p. 094021, 2012.

[17] S. Dastoor and M. Cutkosky, "Design of dielectric electroactive polymers for a compact and scalable variable stiffness device," in *Robotics and Automation (ICRA), 2012 IEEE International Conference on*, May 2012.

[18] J. Newton, J. Morton, J. Clark, and W. Oates, "Modeling and characterization of stiffness controlled robotic legs using dielectric elastomers," in *Proceedings of SPIE 8340*, vol. 83400Z, 2012.

[19] K. Galloway, "Passive variable compliance for dynamic legged robots," Ph.D. dissertation, University of Pennsylvania, 2010.

[20] B. Andrews, B. Miller, J. Schmitt, and J. Clark, "Running over unknown rough terrain with a one-legged planar robot," *Bioinspiration & Biomimetics*, vol. 6, pp. 1–15, Jun 2011.

[21] D. Dudek and R. Full, "Passive mechanical properties of legs from running insects," *Journal of Experimental Biology*, vol. 209, no. 8, pp. 1502–1515, 2006.

[22] M. Daley and A. Biewener, "Running over rough terrain reveals limb control for intrinsic stability," *Proceedings of the National Academy of Sciences*, vol. 103, no. 42, pp. 15 681–15 686, 2006.

[23] J. Schmitt, "A simple stabilizing control for sagittal plane locomotion," *Journal of Computational and Nonlinear Dynamics*, vol. 1, no. 4, pp. 348–357, Oct 2006.

[24] I. Uyanik, U. Saranli, and O. Morgul, "Adaptive control of a spring-mass hopper," in *Robotics and Automation (ICRA), 2011 IEEE International Conference on*, May 2011, pp. 2138–2143.

[25] G. Lynch, J. Clark, P. Lin, and D. Koditschek, "A bioinspired dynamical vertical climbing robot," *The International Journal of Robotics Research*, vol. 31, no. 8, pp. 974–996, 2012.

[26] J. Schmitt, "Incorporating energy variations into controlled sagittal plane locomotion dynamics," in *ASME Conference Proceedings*, vol. 2007, no. 4806X. ASME, 2007, pp. 1627–1635.